Available online at www.sciencedirect.com
SCIENCE DIRECT®
Journal of Power Sources 146 (2005) 793–797
JOURNAL OF POWER SOURCES
www.elsevier.com/locate/jpowsour

0.4 Ah class graphite/$LiMn_2O_4$ lithium-ion battery prototypes

Giovanni Battista Appetecchi, Pier Paolo Prosini *

ENEA, IDROCOMB, C.R. Casaccia, Via Anguillarese 301, 00060 Rome, Italy

Available online 25 May 2005

Abstract

0.4 Ah lithium-ion battery prototypes, developed within a national project devoted to development of power sources for consumer applications, have been fabricated and tested. A novel, intrinsically porous, PVdF–HFP/MgO composite separator, capable to be hot-laminated onto PVDF–HFP-based electrodes without losing its ability to retain liquid electrolyte, was developed. The devices were assembled by direct lamination of the components, namely graphite anode tapes, PVDF–HFP/MgO separators and $LiMn_2O_4$ cathode films. The prototypes, formed by a stack of 12 single cells connected in parallel, need no external pressure to maintain contact between the layers. The battery performance was evaluated in terms of capacity, cycle life, energy and power density at different rates. The capability of prototypes to uptake liquid electrolyte was also investigated. The results have indicated the feasibility to scale-up lithium-ion cells to manufacture 0.4 Ah class battery prototypes showing good cycling performance.

Keywords: Porous separator; PVDF–HFP copolymer; MgO filler; Lithium-ion batteries

1. Introduction

Rechargeable lithium-ion batteries are an excellent choice as power sources for consumers and portable electronic devices [1–4], e.g. laptop computers, cellular phones, photodiode arrays, since their high specific energy and power density [5,6]. In the last years large efforts were devoted to replace liquid electrolytes with ionically conducting gel electrolytes [7] or micro-porous liquid-filled electrolyte separators (PVdF-based) [8,9].

Following the latter approach, we developed a novel porous separator based on magnesium oxide (MgO) as filler in a composite polyvinylidenedifluoride–hexafluoropropylene (PVDF–HFP) polymer matrix [10]. The PVDF–HFP/MgO separator can be hot-pressed onto the electrodes without losing its ability to uptake liquid electrolyte. With respect to the Bellcore process [9], the separator does not require plasticizer extraction to form the porous structure [11] since it is assured by MgO filler. In addition, the filler enhances the capability of the separator to retain liquid electrolyte [12]. Tests performed on PVDF–HFP/MgO separator filled with $LiPF_6$-based liquid electrolyte showed an ionic conductivity equal to 4.0×10^{-4} S cm^{-1} at 20 °C and good electrochemical stability up to 4.4 V [10]. PVDF–HFP copolymer was also used as binder for graphite-based anodes and $LiMn_2O_4$-based cathodes that were found to show good compatibility towards the MgO filler [10].

In this scenario, we decided to investigate the feasibility to scale-up lithium-ion cells using PVDF–HFP/MgO porous films as electrolyte separators. In this work we report the construction and the cycling performance of 0.4 Ah class, graphite/$LiMn_2O_4$ lithium-ion battery prototypes, formed by a stack of 12 parallel connected single cells.

2. Experimental

2.1. Porous separator

The separator films as well as the composite electrodes were prepared by following a procedure developed at ENEA [10] and industrially scaled-up by Ferrania S.p.A. The separator is a self-consistent film having thickness and density

* Corresponding author. Tel.: +39 06 3048 6768; fax: +39 06 3048 6357.
E-mail address: prosini@casaccia.enea.it (P.P. Prosini).

0378-7753/$ – see front matter © 2005 Elsevier B.V. All rights reserved.
doi:10.1016/j.jpowsour.2005.03.085

of 45 μm and 1.53 g cm^{-3}, respectively. The separator was dried under vacuum in an oven at 110 °C for at least 1 day prior to use.

2.2. Composite electrodes

MCMB 2528 graphite (80 wt.%, Osaka Gas, Japan) and $LiMn_2O_4$ powder (85 wt.%, Merck, battery grade) were used as the anode and the cathode active material, respectively. Carbon black (5 wt.%, Super P, MMM carbon, Belgium) was used as electronic conductor while PVDF–HFP copolymer (Aldrich) was used as binder. The electrode components were dispersed in cyclohexanone to obtain a homogeneous slurry. The latter was spread over a glass using calibrated slits and the solvent was allowed to evaporate under a hood. The coated films were dried under vacuum at 110 °C for at least 1 day. Copper (45 μm thick) and aluminum (50 μm thick) nets, used as anode and cathode current collectors, were sandwiched between two anode and cathode tapes, respectively. The sandwiches were cold-calendered to reduce the thickness and improve the current collector/electrode adhesion. At the end of the process, the thickness of the bipolar composite electrode tapes (not including the copper or aluminum net) was about 38 μm (anode) and 144 μm (cathode) with an apparent density (mass/volume) of about 2.6 g cm^{-3} (anode) and 2.8 g cm^{-3} (cathode), corresponding to an active material surface area loading of 8.2 mg cm^{-2} (anode) and 31.1 mg cm^{-2} (cathode), approximately. The theoretical capacity values per area unit were 2.7 mAh cm^2 (anode) and 3.4 mAh cm^2 (cathode), considering the MCMB 2528 graphite and the $LiMn_2O_4$ specific capacity equal to 0.33 Ah g^{-1} (reversible) and 0.11 Ah g^{-1}, respectively. The anode/cathode capacity ratio was fixed to about 0.8 since the coulombic efficiency during the first charge/discharge cycle ranged from 80 to 85%.

2.3. Graphite/$LiMn_2O_4$ battery prototypes

The graphite/$LiMn_2O_4$ battery prototypes are formed by a stack of 12 monopolar cells connected in parallel. The cell design, outlined by the sequence Anode/Separator/Cathode, is illustrated in Fig. 1. The sizes of the anode and cathode tapes (4.8 cm × 2.6 cm) were designed to be slightly lower than those of the polymer separators (5.2 cm × 3.0 cm) to avoid accidental short-circuit. The assembly of the battery prototypes has firstly involved the realization of single monopolar cells. The latter were fabricated by hot-pressing an anode tape, a separator film and a cathode tape at 110 °C and 1.5 bar for 3–5 min. Then, the monopolar cells were alternatively overlapped to separator films following the sequence

Anode/Separator/Cathode/(Separator/Anode/Separator/Cathode)$_{11}$.

The thickness of the battery was 4.3 mm. The anode and cathode nets were intimately connected with the corresponding current collectors (tabs) that are formed by a copper (30 μm, anode) and an aluminum (50 μm, cathode) ribbon, respectively. The prototypes were housed in coffee-bag envelopes and a slight excess (2.0 + 2.2 g, see later in the text) of EC (50 wt.%):DMC:$LiPF_6$ (1 M) solution (Merck, battery grade) was added. The devices were evacuated under moderate vacuum (400–500 mbar) for 1 min to remove most of oxygen and to promote penetration of liquid electrolyte within the battery components. Finally, they were sealed allowing a moderate vacuum inside. The battery assembly and the electrochemical tests were carried out in a controlled atmosphere dry-room (RH < 0.1%, Corridi s.r.l.).

Table 1 reports the weight percent fraction of the components of the graphite/$LiMn_2O_4$ lithium-ion prototypes. The active components of the battery, i.e. anode and cathode tapes, separator foils and liquid electrolyte, represent more than

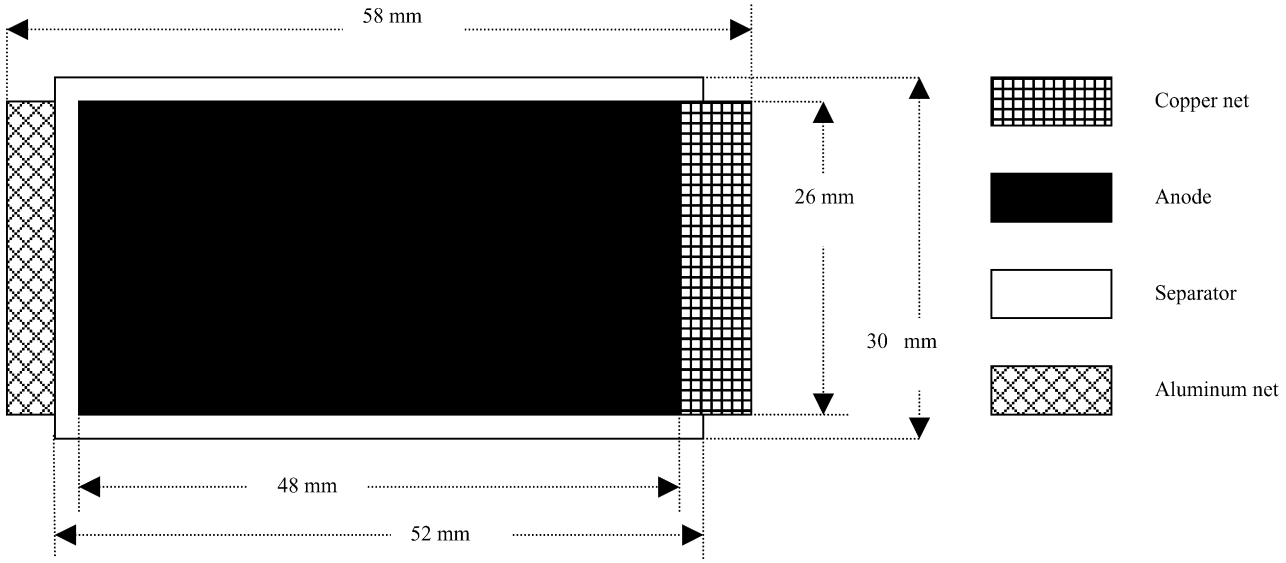

Fig. 1. Cell design of a single graphite/separator/$LiMn_2O_4$ monopolar cell.

Table 1
Weight percent fraction of the components of a 0.4 Ah class, graphite/$LiMn_2O_4$ lithium-ion battery prototypes

Components	wt.%
Anodes	9.2
Separators	17.6
Cathodes	35.3
Current collectors	11.8
Liquid electrolyte	13.1
Packaging	13.0

75% of the weight of the device. The current collector and the packaging contribute to about 25% of the weight. The characteristics of the graphite/$LiMn_2O_4$ battery prototypes are summarized in Table 2. The batteries exhibit a reversible capacity of 0.4 Ah that corresponds to a specific energy of 98 Wh kg^{-1}. The latter was estimated considering an average discharge voltage of 3.7 V and including also the packaging and current collectors weight.

2.4. Dipping tests

The capability of the graphite/$LiMn_2O_4$ battery prototypes to uptake liquid electrolyte was evaluated by adding an excess (7–8 ml) of EC (50 wt.%):DMC:$LiPF_6$ (1 M) solution to liquid-free battery samples and monitoring the weight of the samples as a function of the dipping time. The weight percent increase (ΔW) of battery samples was determined using the equation:

$$\Delta W = \frac{W_S - W_i}{W_i} \times 100 \quad (1)$$

where W_i and W_s represent the weight of the liquid-free battery sample and the weight of the battery sample upon swelling, respectively. The W_i and W_s values do not include the weight of the net substrates, the current collectors and the coffee-bag envelope.

2.5. Electrochemical tests

Impedance measurements were performed using a Solartron Instruments 1260 Impedance Analyzer coupled with a Solartron Electrochemical Interface 1287. The ac tests were carried out at 20 °C in the 10 kHz–10 mHz frequency range using a 10 mV perturbation.

The cycling tests were performed by means of a Maccor S4000 battery tester in the 3.0–4.2 V range at discharge current densities ranging from 0.13 mA cm^{-2} (C/10) to 2.5 mA cm^{-2} (2C). The batteries were always charged using the same procedure to insure identical initial conditions. A constant current step (from 0.1 to 2.0 mA cm^{-2}) was applied up to 4.2 V, followed by a constant voltage step until the current fell below 10% of the nominal value.

Table 2
Characteristics of the graphite/$LiMn_2O_4$ lithium-ion battery prototypes

Size (cm)	58 × 30 × 4.3
Weight (g)[a]	15.3
Active area (cm^2)	287
Reversible capacity (Ah)	0.4
Specific energy (Wh kg^{-1})[a]	98

[a] Packaging and current collectors weight included.

3. Results and discussion

The results of the dipping tests carried out on graphite/$LiMn_2O_4$ lithium-ion prototypes are reported in Fig. 2. A weight increase equal to 26% is observed at the equilibrium reached after 1.5 h dipping. This result was confirmed by impedance measurements, as shown in the insert of Fig. 2, since no feature change was observed upon 1.5 h soaking. A moderate vacuum was found to promote the liquid electrolyte absorption within the battery prototype. In accordance with the data reported in Table 1 the liquid electrolyte content corresponds to 13% of the weight of the device, e.g. considering the weight of the electrode substrates, the current collectors, and the battery packaging.

The voltage/capacity profile of various 0.4 Ah class, graphite/$LiMn_2O_4$ battery prototypes during the first charge/discharge cycle is plotted in Fig. 3A. The tests were carried out at low charge current density, i.e. 0.05 mA cm^{-2}, to promote slow lithium intercalation within the graphite anodes. The prototypes displayed very similar voltage profiles, thus indicating high reproducibility of the manufacturing process. As expected, the first charge step shows a series of plateau in the 3.0–3.8 V range due to the growth of a passive layer onto the graphite anode related to electrolyte decomposition [13]. This was confirmed by gas formation within the device during the first charge. The prototypes were again evacuated and sealed prior the following tests. A 0.4 Ah capacity, i.e. about 100% of the theoretical value, was delivered during the first discharge step with a coulombic efficiency close to 80%. Fig. 3B shows ac responses of

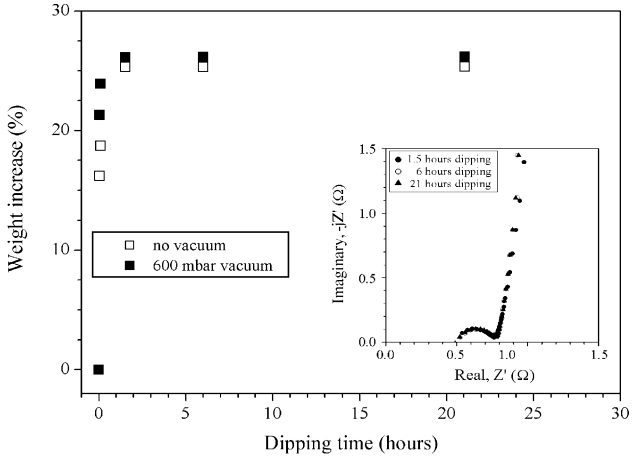

Fig. 2. Weight percent increase vs. soaking time for graphite/$LiMn_2O_4$ lithium-ion battery prototypes in EC (50 wt.%):DMC:$LiPF_6$ (1 M) solution at 20 °C. The insert in the figure reports ac responses taken on the battery samples at different dipping times. Frequency range: 10 kHz–10 mHz.

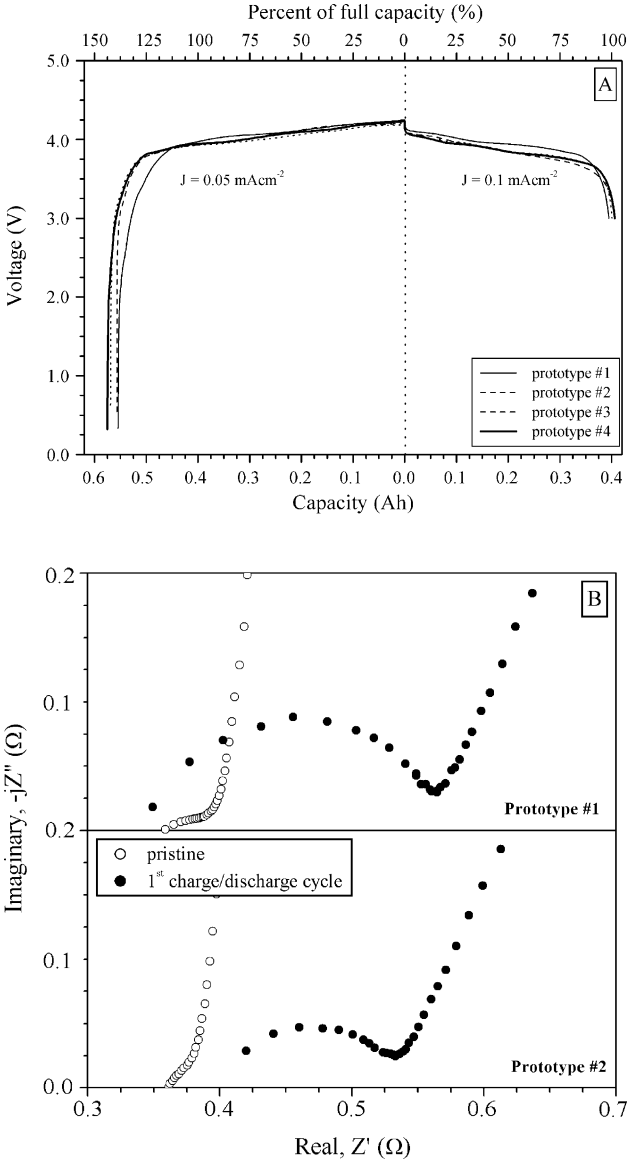

Fig. 3. Panel A: voltage/capacity profile of 0.4 Ah class, graphite/$LiMn_2O_4$ battery prototypes at 20 °C during the first charge/discharge cycle. Current density: 0.05 mA cm^{-2} (charge) and 0.1 mA cm^{-2} (discharge). Panel B: ac responses of 0.4 Ah class, graphite/$LiMn_2O_4$ lithium-ion battery prototypes as built and after the first charge/discharge cycle. Frequency range: 10 kHz–10 mHz.

graphite/$LiMn_2O_4$ battery prototypes as built and after the first charge/discharge cycle. The pristine batteries exhibited resistance values lower than 0.4 Ω. A feature change was observed upon the first charge/discharge cycle with a substantial increase of the interfacial resistance in accordance with the formation of a passive layer onto the graphite anode. The battery resistance upon the first cycle was found to be lower than 0.55 Ω that corresponds to an ohmic drop of 100 mV at C/2 (about 0.16 A), in good agreement with the cycling tests (not reported here).

The Ragone plot of a scaled-up, 0.4 Ah class graphite/$LiMn_2O_4$ battery prototype at 20 °C is illustrated in Fig. 4. At low rates (≤0.13 mA cm^{-2} at C/10)

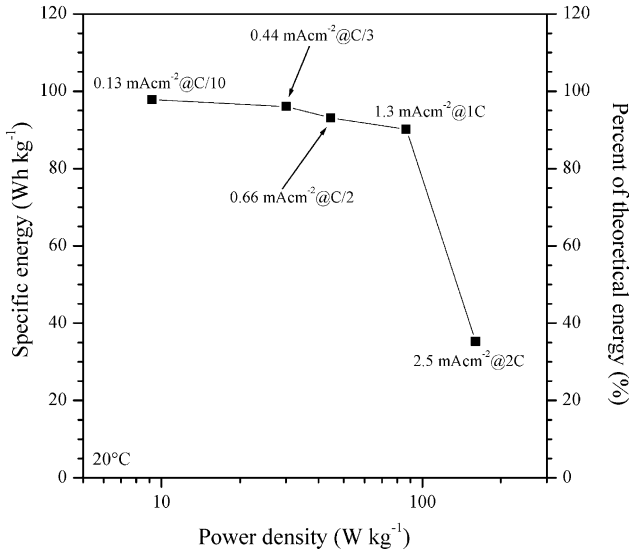

Fig. 4. Ragone plot of a 0.4 Ah class, graphite/$LiMn_2O_4$ battery prototype at 20 °C. The discharge rates and current densities are also reported.

the prototype delivers a specific energy higher than 97.8 Wh kg^{-1}, i.e. more than 99% of the theoretical value, with a power density of 9.2 W kg^{-1}. The results clearly show the capability of the prototype to supply almost the full energy, i.e. more than 92%, up to 1.3 mA cm^{-2} (1C) with a current increase factor of 10, thus enhancing the power density from 9.2 to 86.7 W kg^{-1}. This is of particular interest since consumer applications require high power energy densities. About 36% of the theoretical energy is still delivered at 2.5 mA cm^{-2}, corresponding to a 2C rate while the power density increases up to 160 W kg^{-1}.

The cycling behavior of a scaled-up, 0.4 class, graphite/$LiMn_2O_4$ battery prototype at increasing charge current densities from 0.1 to 2.0 mA cm^{-2} is displayed in Fig. 5. The discharge current density was fixed to 0.2 mA cm^{-2} (C/7). An initial capacity close to 0.4 Ah, i.e. about 100%

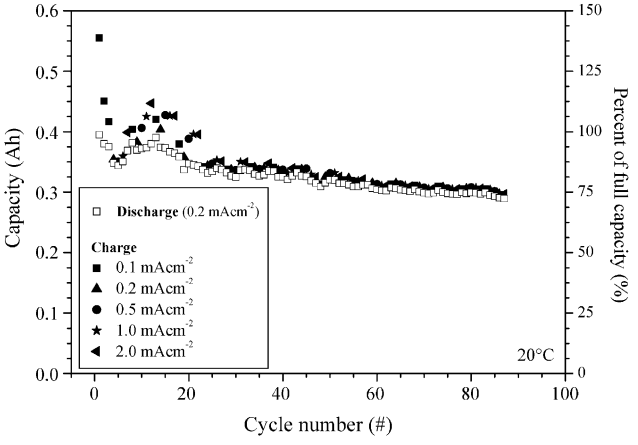

Fig. 5. Capacity vs. cycle number behavior of a 0.4 Ah class, graphite/$LiMn_2O_4$ battery prototype during consecutive cycles at increasing charge current densities (see legend). Discharge current density: 0.2 mA cm^{-2}. $T = 20$ °C.

of the theoretical value, was delivered that progressively decayed to 0.3 Ah after about 90 charge/discharge cycles with a fade lower than 0.3% per cycle. The capacity fade is close to the fading reported for deeply discharged, commercial $LiMn_2O_4$-based cathodes [14]. Therefore, the performance decay could be associated with the intrinsic capacity fading of $LiMn_2O_4$ material rather than to PVDF–HFP/MgO-based electrolyte misbehavior and/or cell design. No relevant effect on the delivered capacity due to the charge rate was observed. This is particularly relevant since lithium-ion batteries for consumers require fast charge times.

4. Conclusions

Graphite/$LiMn_2O_4$ lithium-ion cells for consumer applications, using porous PVDF–HFP/MgO composite separator, have been scaled-up to fabricate 0.4 Ah class battery prototypes with a specific energy equal to 98 Wh kg^{-1}, including the weight of the current collectors and the packaging. The electrochemical tests evidenced the feasibility to manufacture lithium-ion battery prototypes showing highly reproducible cycling performance. At low discharge rates the prototypes delivered initial capacity and specific energy close to the theoretical values. At 1C rate (1.3 mA cm^{-2}) the prototypes are still capable to supply more than 92% of the theoretical energy with a power density of 86.7 W kg^{-1}. No relevant effect of the charge rate on the delivered capacity was observed. It was estimated that a careful optimization of the cell design can enhance the gravimetrical energy up to 150 Wh kg^{-1}. Further improvement is obviously expected when replacing the electrode active material with more performing one.

Acknowledgements

Financial contribution from MIUR (Ministero per l'Istruzione, l'Università e la Ricerca) is kindly acknowledged. The authors thank Ferrania S.p.A. and Arcotronics Italia S.p.A. for providing us the composite tapes and the battery housing, respectively.

References

[1] M. Armand, M. Duclot, French Patent 7,832,976, 1978.
[2] M. Armand, J.M. Chabagno, M. Duclot, in: P. Vashishita, J.N. Mundy, G.K. Shenoy (Eds.), Fast Ion Transport in Solids, Elsevier, New York, 1979.
[3] P. Lightfoot, M.A. Metha, P.G. Bruce, Science 262 (1993) 883.
[4] C.A. Vincent, B. Scrosati, Modern batteries, in: An Introduction to Electrochemical Power Sources, 2nd ed., Arnold, London, 1997.
[5] T. Osaka, Electrochem. Soc. Interface 8 (3) (1999) 9.
[6] Primary and Rechargeable Battery Seminar, Florida Educational Seminars Inc., Fort Lauderdale, FL, 2000.
[7] K.M. Abraham, in: B. Scrosati (Ed.), Applications of Electroactive Polymers, Chapman and Hall, London, 1993.
[8] E. Tsuchida, H. Ohno, K. Tsunemi, Electrochim. Acta 28 (1983) 591.
[9] A.S. Gozdz, C.N. Schumtz, J.-M. Tarascon, P.C. Warren, US Patent 5,418,091, 1995.
[10] P.P. Prosini, P. Villano, M. Carewska, Electrochim. Acta 48 (2002) 227.
[11] A. Du Pasquier, G.G. Amatucci, I. Plitz, T. Zheng, A.S. Gozdz, J.-M. Tarascon, Solid State Ionics 135 (2000) 249.
[12] G.B. Appetecchi, P. Romagnoli, B. Scrosati, Electrochem. Commun. 3 (2001) 281.
[13] S. Megahed, B. Scrosati, J. Power Sources 8 (1982) 289.
[14] Merck Battery Materials data sheets, $LiMn_2O_4$ SP 30 Selectipur 1.01075.